

# Eco-friendly geopolymer-wood building materials: Interactions between geopolymer and wood cell wall

Hanzhou Ye<sup>a,b,c</sup>, Bright Asante<sup>c</sup>, Goran Schmidt<sup>d</sup>, Andreas Krause<sup>d</sup>, Yang Zhang<sup>b,\*</sup>, Zhiming Yu<sup>b</sup>

<sup>a</sup> International Centre for Bamboo and Rattan, Beijing, 100102, China

<sup>b</sup> Ministry of Education Key Laboratory of Wooden Material Science and Application, Beijing Forestry University, Beijing, 100083, China

<sup>c</sup> Institute of Wood Science, University of Hamburg, Hamburg, 21031, Germany

<sup>d</sup> Institute of Wood Research, Johann Heinrich von Thünen Institute, Hamburg, 21031, Germany

## ARTICLE INFO

Handling editor: Zhen Leng

### Keywords:

Geopolymer  
Wood  
Cell wall  
Interaction  
Nanoindentation  
Nanoscratch

## ABSTRACT

Interactions between geopolymer and wood cell wall was investigated to better understand the bonding mechanism of geopolymer-wood composites as sustainable building materials. Elemental distributions, topological chemistry, and micro-mechanical properties between geopolymer and spruce wood cell wall were mainly investigated by the scanning electron microscopy-energy dispersive X-ray spectroscopy (SEM-EDS), UV microspectrophotometry (UMSP), nanoindentation, and nanoscratch. It was discovered that lignin may migrate from the wood cell wall to the surface of the geopolymer and thereafter partially contribute to the production of the geopolymer without appreciably damaging the wood cell wall. Geopolymer mineralized and hardened the surfaces of wood cell walls (S3 and S2 layers) evidenced by the increasing  $H/E$  and  $H^3/E^2$  from spruce cell walls to geopolymer. The average width of the interaction region was around 7.65  $\mu\text{m}$  according to different friction coefficients.

## 1. Introduction

Geopolymer has emerged as an eco-friendly alternative to ordinary Portland cement (OPC) due to its low CO<sub>2</sub> emissions, exemplary durability, excellent loadbearing and compressive strength during high thermal conditions, and brilliant chemicals or acid resistance (Luhar and Luhar, 2022; Paruthi et al., 2022). Wood materials have the merits of natural abundance, recyclability, low cost, low density, excellent mechanical properties, and nontoxicity (Parameswaranpillai et al., 2022). The combination of geopolymer and wood has the potential to provide a multitude of advantages, both in terms of economic and environmental benefits. This combination of geopolymer and wood can help create sustainable and efficient building materials, while preserving the environment. Thus, researches of geopolymer-wood composites in sustainable construction and building materials is becoming increasingly widespread. Maximizing the performance of geopolymer and wood, two environmentally friendly materials, through the use of reduced quantities, more environmentally friendly approaches, lower carbon emissions, and simplified yet effective methods, is crucial for harnessing the

full potential of their composite system. This optimization process aims to show the advantages that arise from the combination of geopolymer and wood, guiding the fabrication and optimization of composite materials, and facilitating the development of green and clean construction materials. The significance of these efforts lies in their potential to expand the application of both materials in sustainable and environmentally friendly construction practices.

The composites of wood materials and geopolymers can be mainly divided into two basic modes in the sustainable construction and building materials field. The geopolymer matrix is either reinforced by natural fibers derived from wood, bamboo, hemp, cotton, jute, sisal, flax, coir, ramie, etc. to encounter the brittleness problems of geopolymers (Kuqo et al., 2023; Gholampour et al., 2022; Zhao et al., 2022). Alternatively, geopolymers function as the inorganic binder in wood-based panels. Compared to commonly used organic adhesives in the wood industry such as phenol-formaldehyde resins and urea-formaldehyde resins, geopolymer inorganic adhesives exhibit low environmental impact, no formaldehyde release, and demonstrate improved flame retardation. The interface between geopolymer and

\* Corresponding author.

E-mail address: [bjfuzhangyang@bjfu.edu.cn](mailto:bjfuzhangyang@bjfu.edu.cn) (Y. Zhang).

<https://doi.org/10.1016/j.jclepro.2023.138381>

Received 8 January 2023; Received in revised form 13 June 2023; Accepted 7 August 2023

Available online 9 August 2023

0959-6526/© 2023 Elsevier Ltd. All rights reserved.

wood material is common structure in all geopolymer-wood composites regardless of the composite structure. However, the interface is usually the weakest part of geopolymer-wood composites due to the different natures between geopolymer (an inorganic material) and wood (an organic material). The investigation revealed a notable reduction in the mechanical strength of the geopolymer-wood composites, primarily attributed to the insufficient interfacial bonding between the geopolymer and high-content wood flour (10-20 wt%) (Ye et al., 2018a). Performance of plant fiber-geopolymer composites could be optimized by manipulating the bonding condition between plant fiber and geopolymer and by refining the properties of the interfacial layer connecting the fiber and matrix (Liu and Lv, 2022).

Investigations of the geopolymer and wood interactions play a key role in the further enhancement of the mechanical properties of geopolymer-wood composites, as the interface is critical for composite performance. Wood is a typical biomass material with three-dimensional pore structures. It has been reported that the performance of wood-adhesive bondlines subjected to stresses will depend on the micro- and nano-scale interactions of the wood and adhesive in the bonded interphase by the gross penetration and cell wall penetration, respectively (Jakes et al., 2019; McKinley et al., 2018). Interconnected pores in the wood structure act as channels for the geopolymer paste to flow in. Thus, gross penetration of geopolymer paste is easily achievable and promoting mechanical interlocking refers to filling into the porous wood structure such as lumens, pits, voids, and cracks. Whether geopolymer serves as the matrix for composite materials or as the inorganic adhesive for wood-based composites, there exists filling of wood cell lumens with geopolymer. Nowadays, the studies on the interactions as interface properties between geopolymer and wood usually based on the gross penetration analyses at a multi-cell scale (Ye et al., 2021; Pan et al., 2020; Sarmin et al., 2020). It was found that the diffusion of potassium or sodium derived from geopolymer paste to wood (Gouny et al., 2012; Pan et al., 2020). A weak interfacial bonding was detected between high-content wood flour and geopolymer in our previous works (Ye et al., 2018a). Moreover, the debonding was observed between geopolymer and wood mainly due to the swelling and shrinkage phenomena of wood during curing process (Gouny et al., 2013). It was reported that the interfacial bonding strength between wood and geopolymer was slightly lower than between wood and urea-formaldehyde resin under dry conditions (Bahrami et al., 2019; Shalbafan et al., 2017).

With the geopolymer filling the wood cell lumens, a distinct interaction region at a smaller scale is formed between the geopolymer and the wood cell wall. The bonding property between wood and adhesive could be significantly improved by the ability of the adhesive to permeate into the cell wall and create a stronger bonding property with the cell wall (Paris and Kamke, 2015; Singh et al., 2008; Chandler et al., 2005). It has been suggested that cell wall penetration can also strengthen the cells and be more resistant to shrinkage and swelling due to the combined qualities of the wood material and adhesive (McKinley et al., 2018). Under the action of geopolymer pastes, mineralization of fibre cell wall as well as deteriorations of lignin and hemicellulose occurred in plant fibres (Assaedi et al., 2017). Current research on the interactions between geopolymer and plant materials is primarily focused on the properties between geopolymer and the porous structure of plant materials, without delving into the analysis of wood cell wall at the smaller scale level. At this level, there already exist inherent material differences between geopolymer and wood. Nevertheless, the characteristics and the mechanisms of interactions between geopolymer and wood cell wall, and the extent of these interactions remain unclear.

This study aims to investigate the properties and interactions between geopolymer and wood cell wall via analyses of elemental distributions, topological chemistry, and micro-mechanical properties. The scanning electron microscopy-energy dispersive X-ray spectroscopy (SEM-EDS), UV microspectrophotometry (UMSP), nanoindentation, and nanoscratch tests were applied. The width of interaction region was then estimated by the sigmoidal curve fitting based on the difference of

friction coefficient between geopolymer and wood cell wall. The findings of this work might significantly increase knowledge of the geopolymer and wood materials interaction, as well as give essential theoretical foundation for better production of geopolymer-wood composites that could serve as clean and sustainable construction materials.

## 2. Experimental section

### 2.1. Materials

Norway spruce (*Picea abies*) radial veneer derived from southern Germany with a thickness of 1.2 mm was supplied by the Eggers Jan Furniergroßhandlung (Hamburg, Germany). The wood dust created on the veneers surface after sanding were removed by compressed air. Metakaolin (MK, MetaMax, BASF, Germany) with 54.59% SiO<sub>2</sub> and 43.03% Al<sub>2</sub>O<sub>3</sub>, sodium silicate (Na<sub>2</sub>SiO<sub>3</sub>) solution (Betol 50T, Ludwigshafen, Germany), and sodium hydroxide (NaOH) pellets with 98.0% purity were used for geopolymer synthesis. The alkaline activator for geopolymer consisted of Na<sub>2</sub>SiO<sub>3</sub> and 10 M NaOH solutions with a 1.33 M ratio of SiO<sub>2</sub>/Na<sub>2</sub>O. The geopolymer paste was obtained by mixing MK and the activator solution. The detailed preparations of alkaline activator and geopolymer paste were described in our previous studies (Ye et al., 2018a, 2018b).

### 2.2. Pretreatments of spruce veneer

Both front and back surfaces of the spruce veneer were sanded to 1 mm thick by a sanding machine (Bütfering Schleiftechnik GmbH, Germany) equipped with 180-grit sandpaper. The wood veneers were cut to the same size (117 mm × 20 mm × 1 mm) and stored in the climate chamber (Pharma 1300, Weiss Technik, Germany) at 20 ± 2 °C and 65 ± 5% relative humidity (RH) for at least 2 weeks before using. The detailed descriptions were available in our previous studies (Ye et al., 2021).

### 2.3. Preparations of the geopolymer-wood composites

Geopolymer paste (320 ± 5 g) was poured into an open cylindrical plastic mold with a diameter of 50 mm and a height of 100 mm. Spruce veneer was embedded vertically into the geopolymer paste at a depth of 50 mm to prepare the samples at ambient temperature and pressure. The samples were cured under 20 ± 2 °C and 65 ± 5% RH for 7 days. The cross-sections of the spruce veneer with geopolymer in the lumens were cut at a distance of 2 mm from the impregnated end of the spruce veneer.

### 2.4. Epoxy resin embedding treatment

Samples were embedded in epoxy resin for the UMSP, nanoindentation, and nanoscratch. The samples for embedding (5 mm × 1 mm × 1 mm) were cut from the geopolymer-wood sample. The cross-sections of the samples were cut and shaped with a blade on the microscope workbench. Five replicate samples were used for each group. Samples were embedded in epoxy resin using the Spurr method (Spurr, 1969) under vacuum at 20 ± 2 °C for 10 min three times by using fresh epoxy resin each time. Finally, the embedded samples were transferred into a plastic mold and dried in the oven at 70 °C for 24 h.

### 2.5. Characterizations

#### 2.5.1. SEM-EDS

For morphology and distribution analysis between geopolymer and wood cell wall by the SEM-EDS, the position at 2 mm above the bottom end of the embedded wood veneers was used. Cross-sections of the untreated spruce and geopolymer-filled spruce specimens were prepared by a microblade. The images and element analysis of the samples (3 mm × 3 mm) were examined by scanning electron microscopy (SEM, LEO

1525, Oberkochen, Germany) equipped with an Octane-Plus™ silicon drift energy dispersive X-ray detector. For the SEM images, samples were coated with platinum (Pt) and analyzed under a high vacuum with 5-kV at an accelerating voltage of 20 kV for the SEM-EDS line scans and elemental mappings.

### 2.5.2. UMSP

Samples for the topological chemistry analysis were investigated by the UMSP (UMSP 80, Carl Zeiss, Oberkochen, Germany) equipped with the APAMOS® scanner. Samples were cut from the cross-section of the resin-embedded geopolymer-wood composites and then cut into 1 μm thin slices by an Ultra-microtome. One tissue sample slice was positioned between two quartz microscope slides, and one drop of glycerin was used to embed the tissue slice. Five slices of samples were collected for each group. The scanning UV wavelength of the UMSP was set at 280 nm, and at least three regions were selected per sample. The details of sample preparation for the UMSP were described in the literature (Koch and Kleist, 2001; Lanvermann et al., 2013).

### 2.5.3. Nanoindentation

Nanoindentation was performed by a Triboindenter (Bruker Hysitron TI 980, Minneapolis, USA). The surface of geopolymer-wood composite samples was polished by the Ultra-microtome after epoxy resin embedding treatment. The Berkovich indenter was loaded into the sample surface in a load-controlled mode for the nanoindentation test. The collection points of nanoindentation, as shown in Fig. S1, were obtained by scanning probe microscopy (SPM) mode via nanoindenter and located on the surface of (a) geopolymer, (b) geopolymer at the interaction region (geopolymer\_i), (c) spruce cell wall at the interaction

region (spruce\_i), and (d) spruce cell wall, respectively. Five points were collected in each area. The nanoindentation loading process was the 5-2-5 mode. Specifically, the load was raised from 0 to 200 μN within 5 s at a constant speed of 40 μN/s, and the load was kept at 200 μN for 2 s and constantly decreased from 200 to 0 μN during an additional 5 s.

### 2.5.4. Nanoscratch

Compared with nanoindentation, nanoscratch can obtain continuous properties characteristics of materials. Nanoscratch was also performed by the Triboindenter. The interaction between the indenter and the object is mainly affected by the tangential force ( $F_T$ ) and the normal force ( $F_N$ ) in the nanoscratch test. The edge forward orientation of the Berkovich indenter was adopted with the angle  $\theta = 13.0^\circ$ . The nanoscratch tested area was traversed from the geopolymer and the spruce cell wall. The test parameters of nanoscratch testing for the sample surface are shown in the time-normal load curve (Fig. S2a) and the time-lateral displacement curve (Fig. S2b). The friction coefficient of the tested material is defined as the ratio of  $F_T$  to  $F_N$ . The friction coefficient can be used to differentiate between two materials in contact. The variation of the friction coefficient distinguished different materials or material components. SEM-EDS was used to investigate the morphology and distinguish the components of the samples after nanoscratch.

## 3. Results

### 3.1. Elemental distributions

Elemental analysis and topochemical characterization of a sample can be provided by the SEM-EDS technique (Sun et al., 2011). In this

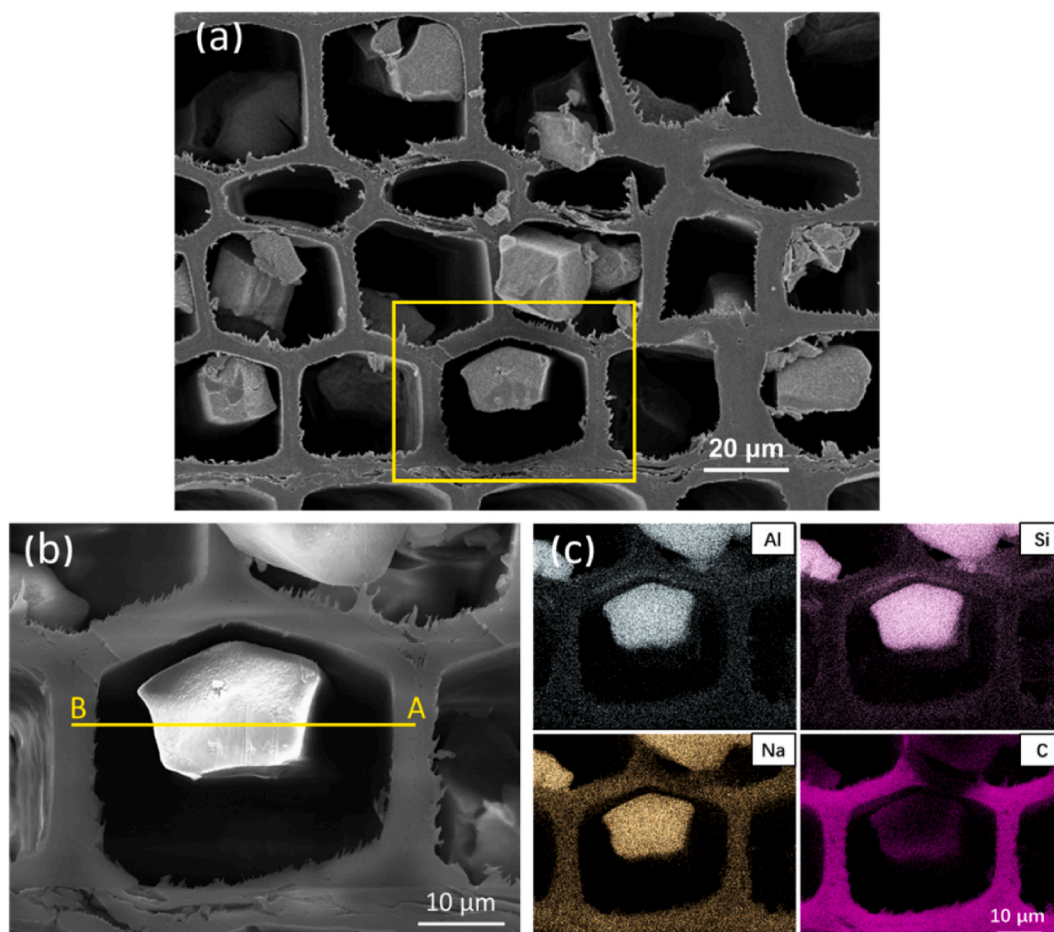


Fig. 1. (a) Geopolymer filled in the wood cell; (b) SEM and (c) SEM-EDS mappings between the wood cell wall and geopolymer.

study, SEM-EDS was applied to investigate the migration and distribution of geopolymer and wood components. It was found that geopolymer filled wood lumens in a variety of ways, either partially (Fig. 1a) or almost fully, creating continuous and discontinuous interaction regions between the geopolymer and the wood cell walls. The typical shape of individual spruce tracheid and the distributions of Al, Si, Na, and C elements at the interaction region of geopolymer and spruce cell wall are shown in SEM-EDS in Fig. 1b and c. SEM-EDS line scanning started from the spruce cell wall (Point A), through geopolymer within the tracheids, and ending at the spruce cell wall (Point B), as shown in Fig. 1b. Different distributions of carbon (C) element was detected in the geopolymer in the SEM-EDS mappings (Fig. 1c) and the SEM-EDS line scans (Fig. 2). It was showed that organic components have migrated from wood into the geopolymer matrix with higher carbon content on the margin and lower content in the center of the geopolymer. Interestingly, low contents of aluminum (Al) and silicon (Si) elements were detected in the wood cell wall. It could be caused by the  $\text{Al}^{3+}$  and  $\text{Si}^{4+}$  ions in the aqueous solution from geopolymer paste penetrating the wood cell wall. Combining the SEM-EDS results and the prevalent partial filling of the geopolymer in the wood cells in Fig. 1a, it can be inferred that the gaps between the geopolymer and the wood cell walls was finally formed due to the initial contact of the geopolymer with the cell walls in a slurry state and filling within the cell walls, but shrinkage occurred with the solidification of geopolymer. This phenomenon of gaps between geopolymers and wood has also been reported in the literature related to the study of the interface between wood and geopolymer (Ye et al., 2021; Gouny et al., 2013).

### 3.2. Topological chemistry

Topological chemistry at the plant cell wall level has been reported to be investigated using the UMSP (Ehmcke et al., 2017), high-resolution AFM (Lou et al., 2021a, 2021b), confocal Raman microscopy (Dai et al., 2022; Jin et al., 2021), etc. In this study, the UMSP was applied to further investigate the interactions between geopolymer and spruce cell walls. Specifically, identifying the carbon-containing substance from the spruce cell wall entering the geopolymer. The UV absorption (280 nm) of the wood cell wall arose from lignin and/or aromatic phenolic compounds (Koch and Kleist, 2001; Wang et al., 2012). The UMSP images of untreated and geopolymer filled individual spruce tracheids are shown in Fig. 3. Different UV absorbance intensities are illustrated by the different color pixels. For instance, blue and grey locations indicate low and high concentrations of UV absorbing components, respectively. The high UV absorption ( $\log \text{Abs}_{280 \text{ nm}} 0.4839$  to  $0.9355$ ) of the compound middle lamellae (CML) and cell corner (CC) was characterized by the

image profiles in both untreated and geopolymer-filled samples. The secondary cell wall had a lower lignin distribution than the CC and CML, consistent with the previous report (Gindl et al., 2004), varying from  $\log \text{Abs}_{280 \text{ nm}} 0.0969$  to  $\log \text{Abs}_{280 \text{ nm}} 0.4194$ . Indeed, lignification is initiated in the central area of the CC and CML (Zeng et al., 2010). A lower lignin concentration with a slight UV absorbance reduction was detected via a combined analysis of color pixels and peak heights at the secondary cell wall, especially the CML, of geopolymer-filled samples (Fig. 3b and d) compared to the untreated samples (Fig. 3a and c). Interestingly, there was a slight UV absorption, shown as blue color pixels, in the geopolymer-filled spruce lumina (Fig. 3b and d). This UV absorption could be related to the alkaline aqua-soluble lignin and/or aromatic phenolic compounds extracted from the wood cell (Korotkova et al., 2015; Jacobs et al., 2002; Lundquist et al., 1983).

### 3.3. Nanoindentation

Nanoindentation was used to investigate the micromechanical properties between geopolymer and the cell wall of spruce tracheids. The load-displacement (P-h) curves of nanoindentation on the surface of geopolymer, geopolymer\_i, spruce\_i, and the spruce cell wall are shown in Fig. 4. The depth of nanoindentation on these four regions increased with the increase of loading. Under the same loading pressure, the indentation depth on the geopolymer surface was the deepest, followed by the geopolymer\_i and the spruce\_i, and finally, the spruce cell wall. The maximum indentation depths were reached on the surface of the material when the applied load reached its maximum of  $200 \mu\text{N}$  and held for 2 s. The unloading stage of the P-h curve reflects the elastic recovery capacity of the materials qualitatively. Steeper curves were detected when the indentations were on the spruce cell wall and spruce\_i, showing a smaller elastic recovery capacity than the geopolymer and the geopolymer\_i. Residual indentation depth is defined as the indentation depth at full unloading, i.e., the loading force is  $0 \mu\text{N}$  at the end of nanoindentation testing. The deeper the residual indentation depth, the smaller the elastic recovery capacity. The relationship between the elastic recovery ability and the maximum indentation depth was consistent with the combined results of the unloading stage shape in the P-h curve and the residual indentation depth in Fig. 4, that is geopolymer  $\approx$  geopolymer\_i  $>$  spruce\_i  $\approx$  spruce cell wall.

A box plot of the nanoindentation hardness ( $H$ ) of geopolymer, geopolymer\_i, spruce\_i, spruce cell wall, and epoxy resin is shown in Fig. 5a. The hardness of the epoxy resin area was tested to investigate the influence of the embedded epoxy resin hardness on the samples. In the nanoindentation test, the embedded resin showed a lower hardness of  $0.25 \text{ GPa}$  with a uniform distribution compared to the other samples. Thus, the effect of embedded epoxy resin on the hardness of the samples could be ignored. Fig. 5a shows that the average hardness of the samples decreased from the surface of geopolymer to the surface of the wood cell wall, reflecting the nanoindentation hardness transition. In detail, the average hardness of geopolymer ( $0.70 \text{ GPa}$ ) was the highest, followed by the geopolymer\_i ( $0.69 \text{ GPa}$ ) and spruce\_i ( $0.59 \text{ GPa}$ ), and the average hardness of spruce cell wall surface ( $0.53 \text{ GPa}$ ) was the lowest. Fig. 5b shows the elastic modulus ( $E$ ) of the geopolymer, geopolymer\_i, spruce\_i, spruce cell wall, and embedded epoxy resin. The embedded epoxy resin elastic modulus was  $4.55 \text{ GPa}$ , lower than other test areas, indicating that the epoxy resin incorporation did not greatly affect the elastic modulus of the samples either. The average elastic modulus of samples decreased from the surface of the spruce cell wall to the geopolymer surface, showing the elastic modulus transition between geopolymer and spruce cell wall. Specifically, the average elastic modulus of the spruce cell wall ( $23.97 \text{ GPa}$ ) was the highest, followed by that of spruce\_i ( $20.67 \text{ GPa}$ ), geopolymer\_i ( $9.90 \text{ GPa}$ ), and finally the geopolymer ( $9.89 \text{ GPa}$ ). Because wood is a natural material with variability in cell locations and the cellulose microfibril angle, the spruce cell wall elastic modulus varied from  $5 \text{ GPa}$  to  $30 \text{ GPa}$  via the nanoindentation method (Konnerth et al., 2009; Gindl et al., 2002, 2004; Wimmer and

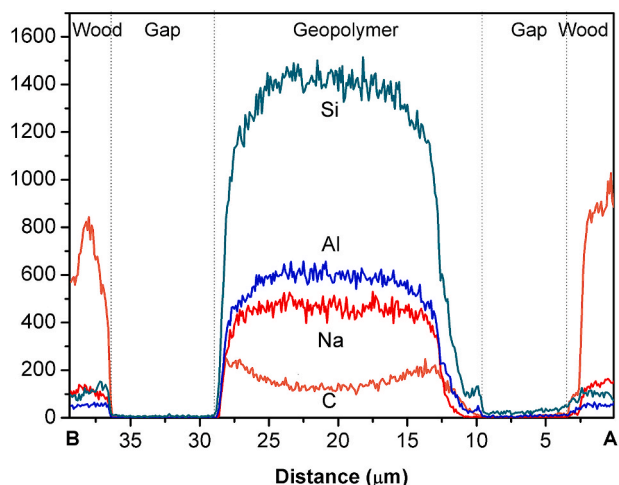


Fig. 2. SEM-EDS line scans between the wood cell wall and geopolymer.

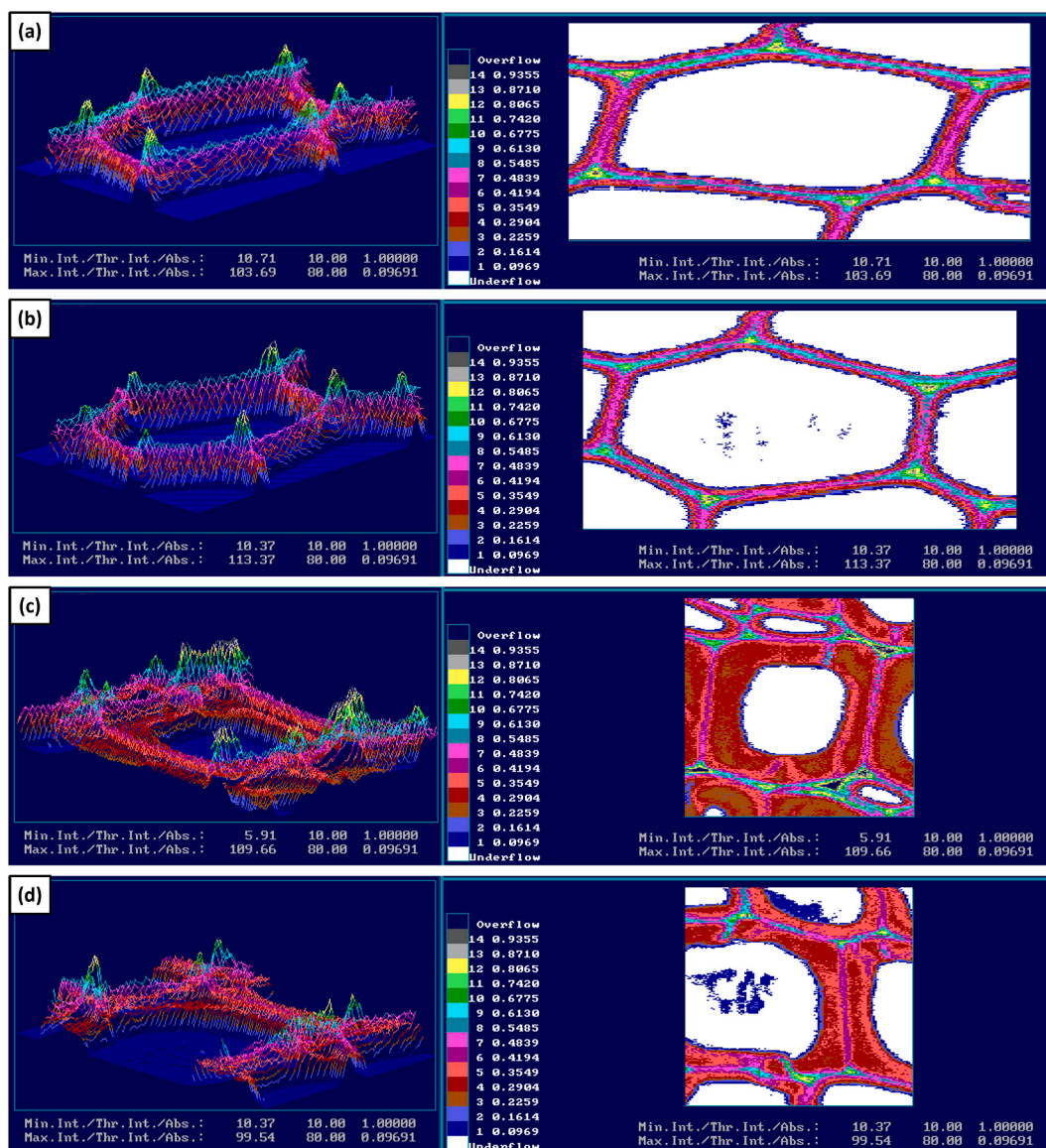


Fig. 3. UMSP images of individual cell wall layers of spruce tracheids measured at  $\lambda_{280\text{nm}}$ : (a) early-wood tracheids, (b) geopolymer-filled early-wood tracheids, (c) late-wood tracheids, and (d) geopolymer-filled late-wood tracheids.

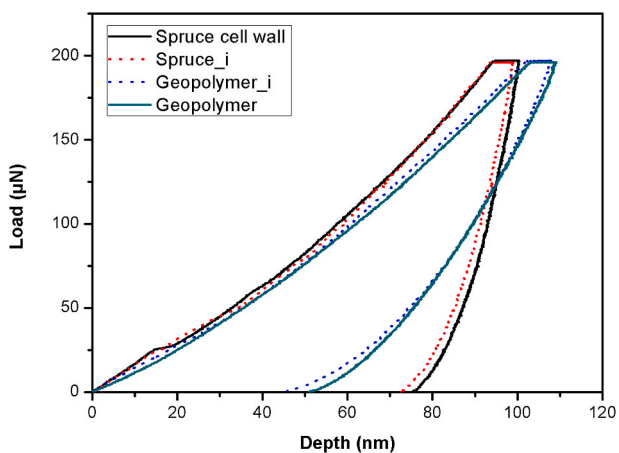


Fig. 4. Load-displacement (P-h) curves from the area between the spruce cell wall and geopolymer.

Lucas, 1997). Similar E for metakaolin-based geopolymers measured by nanoindentation were reported previously (Si et al., 2020; Pelisser et al., 2013). Among them, the geopolymer elastic modulus was smaller than the geopolymer<sub>i</sub>, and the spruce cell wall elastic modulus was close to that of the spruce<sub>i</sub>.

### 3.4. Nanoscratch

SEM images and EDS mappings of sample surface after nanoscratch between geopolymer and spruce are shown in Fig. 6. The red, yellow, blue, and green pixels in the SEM-EDS image in Fig. 6b represented C, Na, Al, and Si elements, respectively. Geopolymer was characterized by Al and Si elements. Spruce cell walls and the embedded epoxy resin were represented by C element. The spruce cell wall could be easily distinguished from the epoxy resin in the SEM image in Fig. 6a. The length of the nanoscratch path from the start point to the end point was 100  $\mu\text{m}$ , and it successively scratched through the blank cell lumen of spruce tracheid, geopolymer-1, cell wall-1, geopolymer-2, cell wall-2, and finally ended in geopolymer-3. In this study, the micromechanical properties of the nanoscratch were analyzed across the area from cell

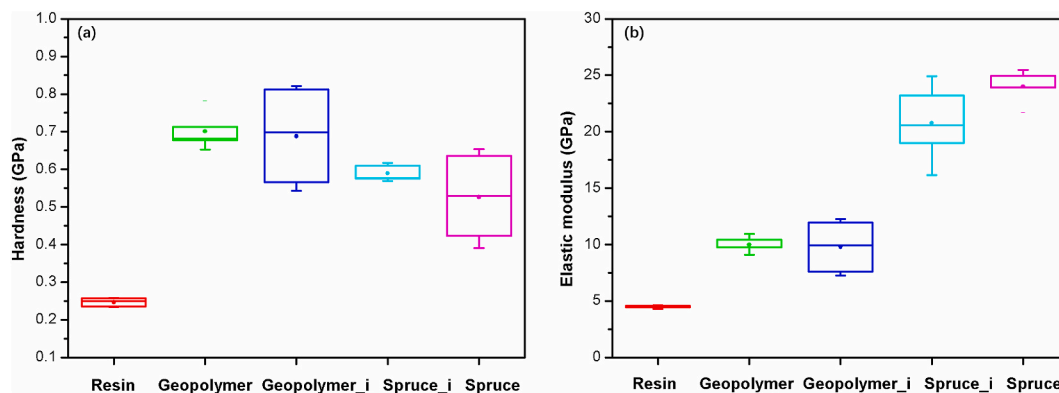


Fig. 5. (a) Nanoindentation hardness and (b) nanoindentation elastic modulus from the area between the spruce cell wall and geopolymer.

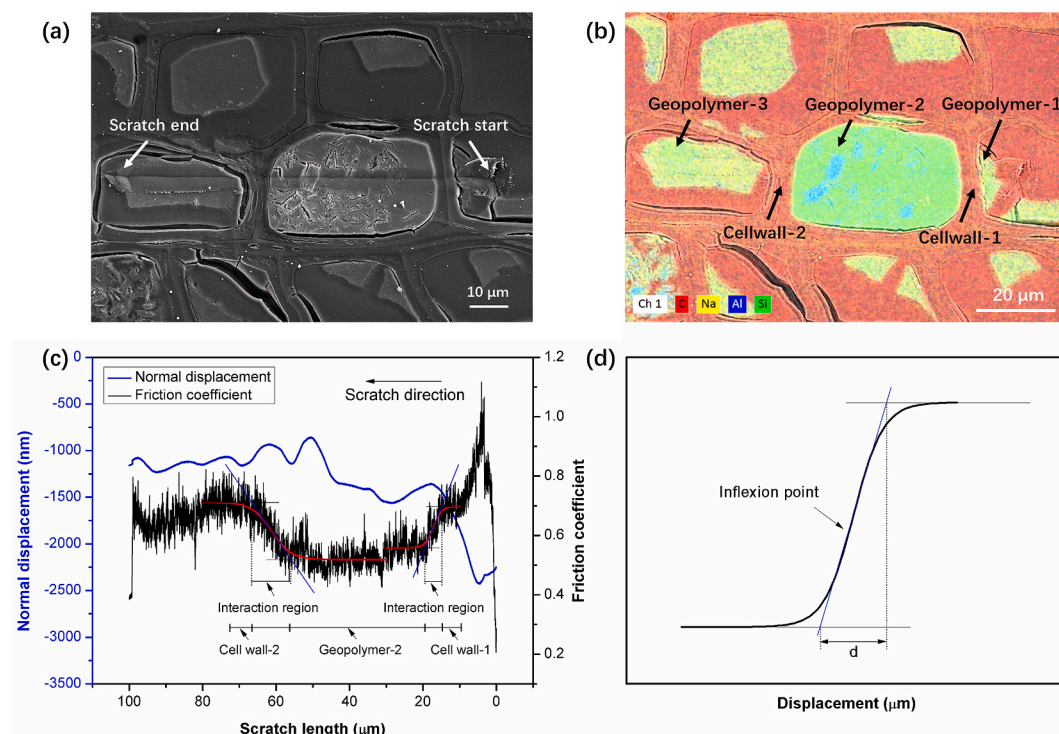


Fig. 6. (a) SEM image and (b) SEM-EDS image of the samples after nanoscratch, (c) the relationships between scratch length and normal displacement/friction coefficient at the interaction region between geopolymer and spruce cell wall, and (d) the width estimation of the interaction region via a sigmoidal curve fitting by drawing a tangent line through the inflexion point of the curve and intersect two baselines.

wall-1 to cell wall-2. The friction coefficient is an important index used to evaluate the micromechanical properties of samples by nanoscratch test. It is considered that the friction coefficient enhancement reflects the interfacial deformation decrease and the interfacial stiffness increase (Janssen et al., 2008). The relationship between the scratch length and friction coefficient/normal displacement is shown in Fig. 6c. The scratch direction was from the right (0 μm) to the left (100 μm) through cell wall-1, geopolymer-2, and cell wall-2 sequentially. Combining the friction coefficient curve in Fig. 6c with the SEM-EDS image of the nanoscratch path in Fig. 6b, the spruce cell walls-1 and cell wall-2 were at around 10 μm and 70 μm, respectively, located at the plateau areas of the friction coefficient curve. The friction coefficient curve between cell walls-1 and cell walls-2 shows a U-shaped region with a scratch length of 10–70 μm at geopolymer-2 adjacent to the spruce cell wall. The average friction coefficient of geopolymer and cell wall was calculated to be 0.5 and 0.7, respectively. The closer the geopolymer was to the spruce cell wall, the greater the friction coefficient.

## 4. Discussion

### 4.1. Effects of wood cell wall on the geopolymer

Effects of wood cell wall on the geopolymer was analyzed by combining the results from the SEM-EDS, nanoindentation, and the UMSP. As the schematic diagram of the intermigration between wood cell components and geopolymer shown in Fig. 7. The spruce tracheid cell wall consists of the middle lamella (ML), CC, primary wall (P), and the outer (S1), middle (S2), and inner layers (S3) of the secondary wall (Adusumalli et al., 2010; Agarwal, 2006). Geopolymer in the spruce tracheid contacted the S3 layer of wood cell wall first when the geopolymer filled the spruce lumen. It was possible to infer that organic wood substances containing lignin and/or aromatic phenolic compounds was mainly distributed at the edges of the geopolymer and rarely existed at its center by combined analyses of the SEM-EDS mapping and line scan and the UMSP results.

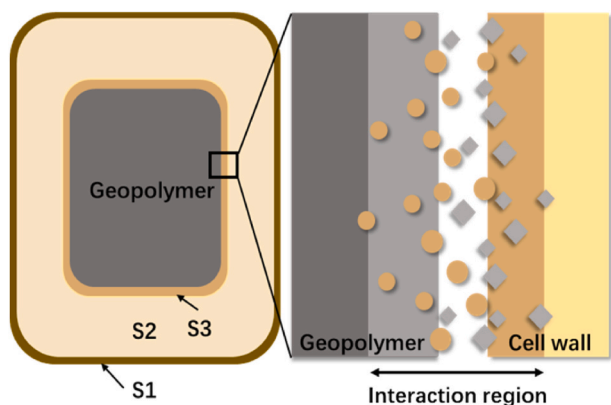


Fig. 7. Schematic of the interactions between geopolymer and wood cell wall.

A conceptual model was developed in the interactions between geopolymer and wood cell wall during the curing process, illustrated in a schematic diagram in Fig. 8. During the geopolymer formation, water participates in the reactions of dissolution, hydrolysis, and polycondensation by acting as a medium for the dissolution of aluminosilicate raw materials, hydrolysis of  $\text{Al}^{3+}$  and  $\text{Si}^{4+}$  compounds, and polycondensation of various dissolved aluminates and silicates (Hajimohammadi et al., 2017; Zuhua et al., 2009). Lignin, the one of the main components of cell wall structure, is the major aromatic phenolic compound in wood. We speculate that lignin released from the wood cell wall, while the solid aluminosilicate components of geopolymer were dissolved in the alkaline system. The released lignin mixed in water and then transferred to the geopolymer paste to participate the geopolymer formation partially. The internal structure of the geopolymer becomes dense, and free water is released onto the geopolymer's surface as a result of geopolymerization (Abdulkareem et al., 2019). It is not conducive to the further penetration of macromolecular phenolic organics in the densified geopolymer structure. Also, the phenolic organics could migrate to the geopolymer surface as free water discharged outward. As a result, the distribution depth of the phenolic organics in the geopolymer was limited, which mainly existed on the surface of the geopolymer but was difficult to the deep inter in the geopolymer structure. As the geopolymerization process continued, water leaked onto the geopolymer surface. In this work, the geopolymer surface serves as both an interaction region between the geopolymer and the wood cell wall. Lignin can act as an improved bonding agent by filling up the voids created by water evaporation. A small amount of lignin addition was beneficial to the mechanical properties of geopolymer in our previous study (Ye et al., 2018b). In the context of the interaction region between wood cell wall and geopolymer, where the wood cell wall material exerted its influence solely on the surface layer of the geopolymer, the impact of wood cell wall material on the micro-mechanical properties of geopolymer could be considered to be minimal.

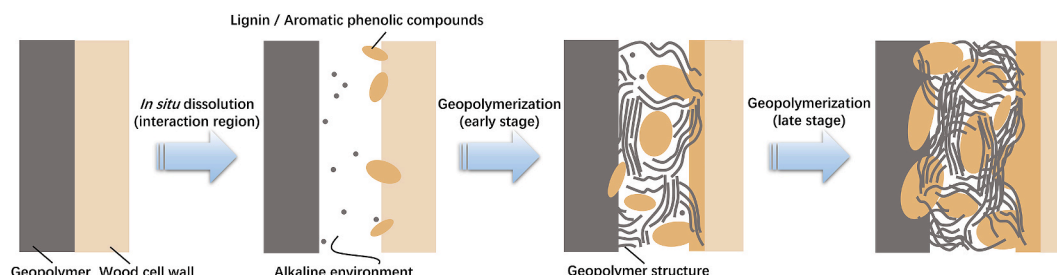


Fig. 8. Schematic of the interactions between geopolymer and wood cell wall during the curing process.

#### 4.2. Effects of geopolymer on the wood cell wall

Effects of geopolymer on the wood cell wall was analyzed by combining the results from the SEM-EDS and nanoindentation. The effects of geopolymer on the wood cell wall could seem to be paradoxically synergistic. On the one hand, the dissolution of  $\text{Al}^{4+}$  and  $\text{Si}^{3+}$  ions from geopolymer leads to mineralization and improvement of wood cell walls. According to earlier research, however, the degradation of plant fiber in an alkaline environment led to a weakening of the link between the plant fiber and the geopolymer matrix, which might ultimately lead to a decrease in the mechanical performance of the composites (Sun et al., 2011). The diffusion depths of  $\text{Al}^{4+}$  and  $\text{Si}^{3+}$  ions in the wood cell wall were estimated to be around 1–2  $\mu\text{m}$  based on the element differences in the SEM-EDS line scan results (Fig. 2). In the wood cell wall, the thickness of S3, S2, S1, P, and ML is around 0.1  $\mu\text{m}$ , 1.0–5.0  $\mu\text{m}$ , 0.1–0.4  $\mu\text{m}$ , 0.1–0.2  $\mu\text{m}$ , and 0.2–1.0  $\mu\text{m}$ , respectively (Agarwal, 2006; Nilsson et al., 2003). It demonstrates that  $\text{Al}^{4+}$  and  $\text{Si}^{3+}$  ions from geopolymer may pass through the S3 layer of the cell wall and into the S2 layer in an entire wood cell. However, it is difficult for  $\text{Al}^{4+}$  and  $\text{Si}^{3+}$  ions to continue to infiltrate deeper regions of wood cell wall, such as S1 layer and P layer, due to the dense cell wall structure and the large range of S2 layer. Thus, the surface (S3 and S2 layers) of wood cell wall was the primary location for the geopolymerization reaction between geopolymer and wood cell wall. In other words, geopolymer mainly acted on the surface of wood cell wall. Degradation of the wood cell wall was extremely limited, as only trace amounts of aromatic phenolic compounds precipitated on the geopolymer surface.

The hardness to elastic modulus ( $H/E$ , elasticity index) and  $H^3/E^2$  based on the nanoindentation results were both used to indicate the toughness and resistance to plastic deformation of materials (Attar et al., 2017; Ehtemam-Haghighi et al., 2017; Coy et al., 2016; Xu et al., 2014; Innocenzi et al., 2001; Leyland and Matthews, 2000). The  $H/E$  and  $H^3/E^2$  ratios of wood cell wall, geopolymer, and their interaction regions were calculated as shown in Fig. 9. The  $H/E$  and  $H^3/E^2$  ratios of spruce and geopolymer were similar to the spruce\_i and geopolymer\_i, respectively. Compared to spruce and spruce\_i, a higher  $H/E$  ratio reflecting elastic recovery with a higher elastic property was detected in the geopolymer and the geopolymer\_i, as shown in Fig. 9a. The  $H^3/E^2$  ratio in Fig. 9b increased gradually from spruce cell wall to geopolymer, consistent with the  $H/E$  ratio. Thus, geopolymer and geopolymer\_i could be defined as the elastic brittle materials as their  $H/E$  ratios were both higher than 0.03 (Innocenzi et al., 2001). Elastic brittle materials, such as concrete, rock, and ceramics, have been reported to fail during loading due to the expansion of micropores and a large number of microcracks in the matrix (Feng and Yu, 1995; Dragon and Mroz, 1979). The  $H/E$  ratios of geopolymer and geopolymer\_i were higher than that of the spruce cell wall and spruce\_i, implying a longer elastic strain to failure of the geopolymer at the interaction region to allow the load redistribution over a large area and delaying the failure of these areas (Xu et al., 2014). The increased  $H/E$  and  $H^3/E^2$  ratios indicate the brittleness enhancement, suggesting that the geopolymer mineralized and then hardened the wood cell wall. Indeed, the release of  $\text{Si}^{4+}$  and  $\text{Al}^{3+}$  ions from geopolymer paste and subsequent deposition in the cell walls

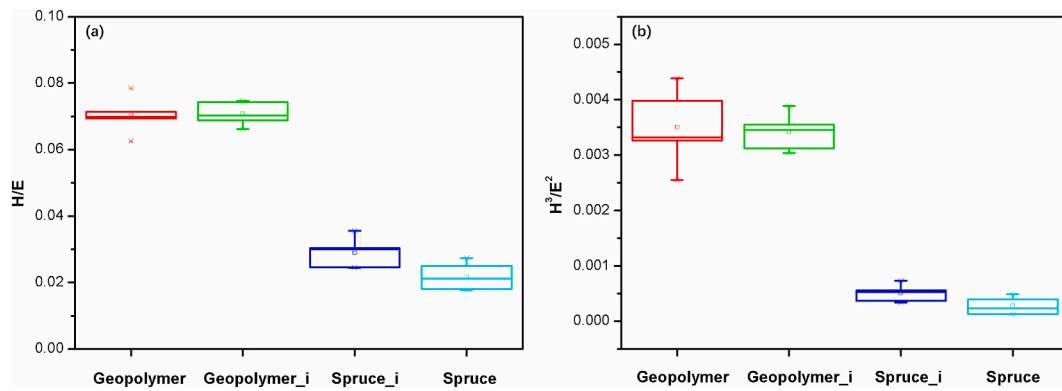


Fig. 9. (a)  $H/E$  and (b)  $H^3/E^2$  from the area between the spruce cell wall and geopolymer.

of wood could be fueled by the alkali erosion of alumina-silicate resource and water's capillary absorption of wood. The impact of geopolymer on the morphology of spruce tracheid cell walls was not prominently observed from the SEM images. Through comprehensive nano-indentation, SEM-EDS, and UMSP topological chemical analysis, it was revealed that geopolymer primarily serves as a mineralization and hardening agent on the surface of the wood cell wall.

#### 4.3. Width of the interaction region

The different friction coefficients of the nanoscratch allow a general distinction between the geopolymer, wood cell walls and their interaction regions. It was detected from Fig. 6c that the friction coefficient of the spruce cell wall was higher than that of the adjacent geopolymer. The geopolymer was identified with the average friction coefficient as 0.539 GPa at the scratch length from 19.50 to 55.84  $\mu\text{m}$ . A similar friction coefficient (0.566 GPa) was reported in the fly ash based geopolymer (Lee et al., 2018). The interaction region between the wood cell wall and the geopolymer was defined around 60 and 10  $\mu\text{m}$  in the scratch curve as shown in Fig. 6c. Moreover, a smooth transition without a cliff-type sudden change was detected from the friction coefficient curve between the spruce cell wall and geopolymer, showing a gradual transition. A tangent line was drawn through the curve's inflection point and intersected with the two baselines based on the difference in friction coefficients between the two materials (Xu et al., 2017). The width of the interaction region could be defined based on the nanoscratch data by a S-shaped fitted curve method shown in Fig. 6d. In this study, the average width of the interaction region between geopolymer and spruce cell wall was around 7.65  $\mu\text{m}$  using the sigmoidal curve fitting method.

#### 5. Conclusions

This study revealed the interactions between geopolymer and spruce wood cell walls mainly by the elemental distributions, topological chemistry, and micro-mechanical properties. A conceptual model was developed in the interactions between geopolymer and wood cell wall during the curing process. It was found that lignin may migrate from the spruce wood cell wall to the surface of the geopolymer and subsequently partially contribute in the creation of the geopolymer without significantly degrading the wood cell wall. Geopolymer mineralized and hardened the surfaces of wood cell walls (S3 and S2 layers) indicated by the gradual increase of the  $H/E$  and  $H^3/E^2$  ratios from spruce cell walls to geopolymer. The average width of the interaction region between the geopolymer and spruce cell wall was around 7.65  $\mu\text{m}$  by a sigmoidal curve fitting based on the difference of friction coefficient.

#### CRedit authorship contribution statement

Hanzhou Ye: Conceptualization, Methodology, Validation,

Investigation, Data curation, Writing – original draft, Writing – review & editing, Funding acquisition, Project administration. **Bright Asante:** Methodology, Investigation, Writing – review & editing. **Goran Schmidt:** Methodology, Writing – review & editing. **Andreas Krause:** Resources, Funding acquisition, Writing – review & editing, Supervision. **Yang Zhang:** Writing – review & editing. **Zhiming Yu:** Writing – review & editing, Supervision.

#### Declaration of competing interest

The authors declare that they have no known competing financial interests or personal relationships that could have appeared to influence the work reported in this paper.

#### Data availability

No data was used for the research described in the article.

#### Acknowledgements

This work was supported by the Fundamental Research Funds for the Central Universities [grant number BFUKF202215], the National Natural Science Foundation of China [grant number 32201644], the China Scholarship Council [No. 201806510025], and the BioHome project funded by the German Federal Ministry of Education and Research (BMBF) [grant number 01DG17007A] and the DAAD project [grant number 57359374].

#### Appendix A. Supplementary data

Supplementary data to this article can be found online at <https://doi.org/10.1016/j.jclepro.2023.138381>.

#### References

- Abdulkareem, O.A., Ramli, M., Matthews, J.C., 2019. Production of geopolymer mortar system containing high calcium biomass wood ash as a partial substitution to fly ash: an early age evaluation. *Compos. Part B-Eng.* 174, 106941 <https://doi.org/10.1016/j.compositesb.2019.106941>.
- Adusumalli, R.-B., Raghavan, R., Ghisleni, R., Zimmermann, T., Michler, J., 2010. Deformation and failure mechanism of secondary cell wall in Spruce late wood. *Appl. Phys. A* 100, 447–452. <https://doi.org/10.1007/s00339-010-5847-1>.
- Agarwal, U.P., 2006. Raman imaging to investigate ultrastructure and composition of plant cell walls: distribution of lignin and cellulose in black spruce wood (*Picea mariana*). *Planta* 224, 1141–1153. <https://doi.org/10.1007/s00425-006-0295-z>.
- Assaedi, H., Shaikh, F., Low, I.M., 2017. Effect of nanoclay on durability and mechanical properties of flax fabric reinforced geopolymer composites. *J. Asian Ceram. Soc.* 5 (1), 62–70. <https://doi.org/10.1016/j.jascer.2017.01.003>.
- Attar, H., Ehtemam-Haghighi, S., Kent, D., Okulov, I., Wendrock, H., Bönisch, M., Volegov, A., Calin, M., Eckert, J., Dargusch, M., 2017. Nanoindentation and wear properties of Ti and Ti-TiB composite materials produced by selective laser melting. *Mater. Sci. Eng. A* 688, 20–26. <https://doi.org/10.1016/j.msea.2017.01.096>.

- Bahrami, M., Shalbafan, A., Welling, J., 2019. Development of plywood using geopolymer as binder: effect of silica fume on the plywood and binder characteristics. *Eur. J. Wood Wood Prod.* 77, 981–994. <https://doi.org/10.1007/s00107-019-01462-3>.
- Chandler, J.G., Brandon, R.L., Frihart, C.R., 2005. Examination of adhesive penetration in modified wood using fluorescence microscopy. In: *ASC Spring 2005 Convention and Exposition, Columbus, OH, USA, 17–20 April 2005. Adhesive and Sealant Council, Bethesda, MD, USA*, p. 10.
- Coy, E., Yate, L., Kabacińska, Z., Jancelewicz, M., Jurga, S., Iatsunskyi, I., 2016. Topographic reconstruction and mechanical analysis of atomic layer deposited Al<sub>2</sub>O<sub>3</sub>/TiO<sub>2</sub> nanolaminates by nanoindentation. *Mater. Des.* 111, 584–591. <https://doi.org/10.1016/j.matdes.2016.09.030>.
- Dai, L., Wang, J., Liu, X.-E., Ma, Q., Fei, B., Ma, J., Jin, Z., 2022. In-situ visualizing selective lignin dissolution of tracheids wall in reaction wood. *Int. J. Biol. Macromol.* 222, 691–700. <https://doi.org/10.1016/j.ijbiomac.2022.09.206>.
- Dragon, A., Mroz, Z., 1979. A continuum model for plastic-brittle behaviour of rock and concrete. *Int. J. Eng. Sci.* 17 (2), 121–137. [https://doi.org/10.1016/0020-7225\(79\)90058-2](https://doi.org/10.1016/0020-7225(79)90058-2).
- Ehmcke, G., Pilgård, A., Koch, G., Richter, K., 2017. Topochemical analyses of furfuryl alcohol-modified radiata pine (*Pinus radiata*) by UMSP, light microscopy and SEM. *Holzforschung* 71 (10), 821–831. <https://doi.org/10.1515/hf-2016-0219>.
- Ehtemam-Haghighi, S., Cao, G., Zhang, L.-C., 2017. Nanoindentation study of mechanical properties of Ti based alloys with Fe and Ta additions. *J. Alloys Compd.* 692, 892–897. <https://doi.org/10.1016/j.jallcom.2016.09.123>.
- Feng, X.-Q., Yu, S.-W., 1995. Micromechanical modelling of tensile response of elastic-brittle materials. *Int. J. Solid Struct.* 32 (22), 3359–3372. [https://doi.org/10.1016/0020-7683\(94\)00305-G](https://doi.org/10.1016/0020-7683(94)00305-G).
- Gholampour, A., Danish, A., Ozbakkaloglu, T., Yeon, J.H., Gencel, O., 2022. Mechanical and durability properties of natural fiber-reinforced geopolymers containing lead smelter slag and waste glass sand. *Construct. Build. Mater.*, 129043 <https://doi.org/10.1016/j.conbuildmat.2022.129043>.
- Gindl, W., Gupta, H., Grünwald, C., 2002. Lignification of spruce tracheid secondary cell walls related to longitudinal hardness and modulus of elasticity using nano-indentation. *Can. J. Bot.* 80 (10), 1029–1033. <https://doi.org/10.1139/b02-091>.
- Gindl, W., Gupta, H., Schöberl, T., Lichtenegger, H., Fratzl, P., 2004. Mechanical properties of spruce wood cell walls by nanoindentation. *Appl. Phys. A* 79, 2069–2073. <https://doi.org/10.1007/s00339-004-2864-y>.
- Gouny, F., Fouchal, F., Maillard, P., Rossignol, S., 2012. A geopolymer mortar for wood and earth structures. *Construct. Build. Mater.* 36, 188–195. <https://doi.org/10.1016/j.conbuildmat.2012.04.009>.
- Gouny, F., Fouchal, F., Pop, O., Maillard, P., Rossignol, S., 2013. Mechanical behavior of an assembly of wood-geopolymer-earth bricks. *Construct. Build. Mater.* 38, 110–118. <https://doi.org/10.1016/j.conbuildmat.2012.07.113>.
- Hajimohammadi, A., Ngo, T., Mendis, P., 2017. How does aluminium foaming agent impact the geopolymer formation mechanism? *Cement Concr. Compos.* 80, 277–286. <https://doi.org/10.1016/j.cemconcomp.2017.03.022>.
- Innocenzi, P., Esposito, M., Maddalena, A., 2001. Mechanical properties of 3-glycidoxypropyltrimethoxysilane based hybrid organic-inorganic materials. *J. Sol. Gel Sci. Technol.* 20, 293–301. <https://doi.org/10.1023/A:1008782203971>.
- Jacobs, A., Lundqvist, J., Ståhlbrand, H., Tjerneld, F., Dahlman, O., 2002. Characterization of water-soluble hemicelluloses from spruce and aspen employing SEC/MALDI mass spectroscopy. *Carbohydr. Res.* 337 (8), 711–717. [https://doi.org/10.1016/S0008-6215\(02\)00054-X](https://doi.org/10.1016/S0008-6215(02)00054-X).
- Jakes, J.E., Frihart, C.R., Hunt, C.G., Yelle, D.J., Plaza, N.Z., Lorenz, L., Grigsby, W., Ching, D.J., Kamke, F., Gleber, S.-C., 2019. X-ray methods to observe and quantify adhesive penetration into wood. *J. Mater. Sci.* 54 (1), 705–718. <https://doi.org/10.1007/s10853-018-2783-5>.
- Janssen, D., Mann, K.A., Verdonshot, N., 2008. Micro-mechanical modeling of the cement–bone interface: the effect of friction, morphology and material properties on the micromechanical response. *J. Biomech.* 41 (15), 3158–3163. <https://doi.org/10.1016/j.jbiomech.2008.08.020>.
- Jin, K., Ling, Z., Jin, Z., Ma, J., Yang, S., Liu, X., Jiang, Z., 2021. Local variations in carbohydrates and matrix lignin in mechanically graded bamboo culms. *Polymers* 14 (1), 143. <https://doi.org/10.3390/polym14010143>.
- Koch, G., Kleist, G., 2001. Application of scanning UV microspectrophotometry to localise lignins and phenolic extractives in plant cell walls. *Holzforschung* 55 (6), 563–567. <https://doi.org/10.1515/HF.2001.091>.
- Konnerth, J., Gierlinger, N., Keckes, J., Gindl, W., 2009. Actual versus apparent within cell wall variability of nanoindentation results from wood cell walls related to cellulose microfibril angle. *J. Mater. Sci.* 44, 4399–4406. <https://doi.org/10.1007/s10853-009-3665-7>.
- Korotkova, E., Pranovich, A., Wärnå, J., Salmi, T., Murzin, D.Y., Willför, S., 2015. Lignin isolation from spruce wood with low concentration aqueous alkali at high temperature and pressure: influence of hot-water pre-extraction. *Green Chem.* 17 (11), 5058–5068. <https://doi.org/10.1039/C5GC01341K>.
- Kuqo, A., Koddenberg, T., Mai, C., 2023. Use of dry mixing-spraying process for the production of geopolymer-bonded wood and seagrass fibreboards. *Compos. Part B-Eng.* 248, 110387. <https://doi.org/10.1016/j.compositesb.2022.110387>.
- Lanvermann, C., Evans, R., Schmitt, U., Hering, S., Niemi, P., 2013. Distribution of structure and lignin within growth rings of Norway spruce. *Wood Sci. Technol.* 47, 627–641. <https://doi.org/10.1007/s00226-013-0529-8>.
- Lee, H., Vimonsatit, V., Chindaprasit, P., Ngo, T., Mendis, P., 2018. Creep properties of cement and alkali activated fly ash materials using nanoindentation technique. *Construct. Build. Mater.* 168, 547–555. <https://doi.org/10.1016/j.conbuildmat.2018.02.166>.
- Leyland, A., Matthews, A., 2000. On the significance of the H/E ratio in wear control: a nanocomposite coating approach to optimised tribological behaviour. *Wear* 246 (1–2), 1–11. [https://doi.org/10.1016/S0043-1648\(00\)00488-9](https://doi.org/10.1016/S0043-1648(00)00488-9).
- Liu, J., Lv, C., 2022. Durability of cellulose-fiber-reinforced geopolymers: a review. *Molecules* 27 (3), 796. <https://doi.org/10.3390/molecules27030796>.
- Lou, Z., Han, X., Liu, J., Ma, Q., Yan, H., Yuan, C., Yang, L., Han, H., Weng, F., Li, Y., 2021a. Nano-Fe<sub>3</sub>O<sub>4</sub>/bamboo bundles/bamboo bundles/phenolic resin oriented recombination ternary composite with enhanced multiple functions. *Compos. Part B-Eng.* 226, 109335. <https://doi.org/10.1016/j.compositesb.2021.109335>.
- Lou, Z., Yuan, T., Wang, Q., Wu, X., Hu, S., Hao, X., Liu, X., Li, Y., 2021b. Fabrication of crack-free flattened bamboo and its macro-/micromorphological and mechanical properties. *J. Renew. Mater.* 9 (5), 959–977. <https://doi.org/10.32604/jrm.2021.014285>.
- Luhar, I., Luhar, S., 2022. A comprehensive review on fly ash-based geopolymer. *J. Compos. Sci.* 6 (8), 219. <https://doi.org/10.3390/jcs6080219>.
- Lundquist, K., Simonson, R., Tingsvik, K., 1983. Lignin carbohydrate linkages in milled wood lignin preparations from spruce wood. *Sven. Papperstidning* 86 (6), 44–47.
- McKinley, P., Kamke, F.A., Sinha, A., De Andrade, V., Jakes, J.E., 2018. Analysis of adhesive penetration into wood using nano-X-ray computed tomography. *Wood Fiber Sci.* 50 (1), 66–76.
- Nilsson, T., Brändström, J., Bardage, S.L., Daniel, G., 2003. The structural organisation of the S1 cell wall layer of Norway spruce tracheids. *IAWA J.* 24 (1), 27–40. <https://doi.org/10.1163/22941932-90000318>.
- Pan, D., Ye, H., Wang, X., Zhang, Y., 2020. Modified geopolymer-based wood adhesive using waterborne polyurethane. *Bioresources* 15 (4), 7573–7585. <https://doi.org/10.15376/biores.15.4.7573-7585>.
- Parameswaranpillai, J., Gopi, J.A., Radoor, S., Dominic, C.M., Krishnasamy, S., Deshmukh, K., Hameed, N., Salim, N.V., Sienkiewicz, N., 2022. Turning waste plant fibers into advanced plant fiber reinforced polymer composites: a comprehensive review. *Compos. Part C-Open Access* 10, 100333. <https://doi.org/10.1016/j.jcocom.2022.100333>.
- Paris, J.L., Kamke, F.A., 2015. Quantitative wood–adhesive penetration with X-ray computed tomography. *Int. J. Adhesion Adhes.* 61, 71–80. <https://doi.org/10.1016/j.jadhadh.2015.05.006>.
- Paruthi, S., Husain, A., Alam, P., Khan, A.H., Hasan, M.A., Magbool, H.M., 2022. A review on material mix proportion and strength influence parameters of geopolymer concrete: application of ANN model for GPC strength prediction. *Construct. Build. Mater.* 356, 129253. <https://doi.org/10.1016/j.conbuildmat.2022.129253>.
- Pelisser, F., Guerrino, E., Menger, M., Michel, M., Labrincha, J., 2013. Micromechanical characterization of metakaolin-based geopolymers. *Construct. Build. Mater.* 49, 547–553. <https://doi.org/10.1016/j.conbuildmat.2013.08.081>.
- Sarmin, S.N., Rahman, W.M.N.W.A., Mohd Yunus, N.Y., Ahmad, N., 2020. Determination of the bond strength of wood veneer and geopolymer matrix by means of a pull-out test. *Mater. Sci. Forum* 981, 162–168. <https://doi.org/10.4028/www.scientific.net/MSF.981.162>.
- Shalbafan, A., Welling, J., Hasch, J., 2017. Effect of aluminosilicate powders on the applicability of innovative geopolymer binders for wood-based composites. *Eur. J. Wood Wood Prod.* 75, 893–902. <https://doi.org/10.1007/s00107-017-1172-0>.
- Si, R., Guo, S., Dai, Q., Wang, J., 2020. Atomic-structure, microstructure and mechanical properties of glass powder modified metakaolin-based geopolymer. *Construct. Build. Mater.* 254, 119303. <https://doi.org/10.1016/j.conbuildmat.2020.119303>.
- Singh, A., Dawson, B., Rickard, C., Bond, J., Singh, A., 2008. Light, confocal and scanning electron microscopy of wood-adhesive interface. *Microsc. Anal.* 22 (3), 5–8.
- Spurr, A.R., 1969. A low-viscosity epoxy resin embedding medium for electron microscopy. *J. Ultra. Res.* 26 (1–2), 31–43. [https://doi.org/10.1016/S0022-5320\(69\)90033-1](https://doi.org/10.1016/S0022-5320(69)90033-1).
- Sun, Y., Mukherjee, A., Kuznetsov, O., Thaner, R., Alemany, L.B., Billups, W., 2011. Functionalization by reductive alkylation and mapping of a subbituminous coal by energy dispersive X-ray spectroscopy. *Energy Fuel.* 25 (4), 1571–1577. <https://doi.org/10.1021/ef200106g>.
- Wang, X.P., Pang, Y.X., Yang, D.J., Lou, H.M., Qiu, X.Q., 2012. Effect of composition of calcium lignosulfonate on setting of Portland cement with anhydrite. *Adv. Mater. Res.* 557–559, 877–882. <https://doi.org/10.4028/www.scientific.net/AMR.557-559.877>.
- Wimmer, R., Lucas, B.N., 1997. Comparing mechanical properties of secondary wall and cell corner middle lamella in spruce wood. *IAWA J.* 18 (1), 77–88. <https://doi.org/10.1163/22941932-90001463>.
- Xu, J., Corr, D.J., Shah, S.P., 2017. Nanoscratch study of the modification effects of nanoSiO<sub>2</sub> on C–S–H gel/cement grain interfaces. *J. Mater. Civ. Eng.* 29 (9), 04017093. [https://doi.org/10.1061/\(ASCE\)MT.1943-5533.0001930](https://doi.org/10.1061/(ASCE)MT.1943-5533.0001930).
- Xu, J., dong Wang, G., Lu, X., Liu, L., Munroe, P., Xie, Z.-H., 2014. Mechanical and corrosion-resistant properties of Ti–Nb–Si–N nanocomposite films prepared by a double glow discharge plasma technique. *Ceram. Int.* 40 (6), 8621–8630. <https://doi.org/10.1016/j.ceramint.2014.01.079>.
- Ye, H., Asante, B., Schmidt, G., Krause, A., Zhang, Y., Yu, Z., 2021. Interfacial bonding properties of the eco-friendly geopolymer-wood composites: influences of embedded wood depth, wood surface roughness, and moisture conditions. *J. Mater. Sci.* 56, 7420–7433. <https://doi.org/10.1007/s10853-021-05775-8>.
- Ye, H., Zhang, Y., Yu, Z., 2018a. Wood flour's effect on the properties of geopolymer-based composites at different curing times. *Bioresources* 13 (2), 2499–2514. <https://doi.org/10.15376/biores.13.2.2499-2514>.
- Ye, H., Zhang, Y., Yu, Z., Mu, J., 2018b. Effects of cellulose, hemicellulose, and lignin on the morphology and mechanical properties of metakaolin-based geopolymer. *Construct. Build. Mater.* 173, 10–16. <https://doi.org/10.1016/j.conbuildmat.2018.04.028>.

- Zeng, Y., Saar, B.G., Friedrich, M.G., Chen, F., Liu, Y.-S., Dixon, R.A., Himmel, M.E., Xie, X.S., Ding, S.-Y., 2010. Imaging lignin-downregulated alfalfa using coherent anti-Stokes Raman scattering microscopy. *Bioenerg. Res.* 3, 272–277. <https://doi.org/10.1007/s12155-010-9079-1>.
- Zhao, J., Trindade, A.C.C., Liebscher, M., de Andrade Silva, F., Mechtcherine, V., 2022. A review of the role of elevated temperatures on the mechanical properties of fiber-reinforced geopolymer (FRG) composites. *Cement Concr. Compos.* 137, 104885. <https://doi.org/10.1016/j.cemconcomp.2022.104885>.
- Zuhua, Z., Xiao, Y., Huajun, Z., Yue, C., 2009. Role of water in the synthesis of calcined kaolin-based geopolymer. *Appl. Clay Sci.* 43 (2), 218–223. <https://doi.org/10.1016/j.clay.2008.09.003>.